Integration of Photonic Crystals into Flexible Dye Solar Cells: A Route toward Bendable and Adaptable Optoelectronic Devices Displaying Structural Color and Enhanced Efficiency

*Yuelong Li, Mauricio E. Calvo, and Hernán Míguez**

Herein is presented what is believed to be the first example of integration of photonic structures in a flexible optoelectronic device. The resulting devices may be designed to display any color in the visible range and, simultaneously, present enhanced power conversion efficiency as a consequence of the increased light harvesting caused by the colored back reflection. The achievement results from the incorporation of nanoparticle-based multilayers with photonic crystal properties that are modified to be compatible with the chemical and physical processing of flexible nanocrystalline titania electrodes of dye solar cells. The photovoltaic performance of these colored flexible cells remains unaltered after one hundred bending cycles, thus showing the high-mechanical stability of the ensemble. These devices reunite most characteristics required for building integration or for the construction of solar window panes, such as light weight, stability upon bending, adaptability, and color. This work may trigger promising applications of these highly adaptable and versatile photonic crystals in other flexible devices.

1. Introduction

Flexible photovoltaics (PV) have attracted tremendous attention in recent years[1–10] since it constitutes an alternative clean energy source that combines low-cost, light-weight, and high-efficiency. The most promising applications of flexible solar cell devices are found in the fields of building integrated photovoltaics (BIPV) and of portable energy sources for rechargeable devices.[1,4] In both cases, the PV solution applied should be aesthetically attractive, with the possibility to present the desired color and a certain degree of transparency if required; versatile, in terms of its adaptability to different surfaces; and of the lowest possible weight, as it should not add load to walls, facades, or roofs, nor to the devices to be charged. In this regard, flexible dye solar cells (DSCs) present the potential to show many of these features. While their low weight and adaptability have been repeatedly demonstrated,[11–13] their color and transparency have been hardly addressed. In fact, in order to enhance the efficiency of these devices, working electrodes often include diffuse scattering particles that improve light-harvesting efficiency, but that unfortunately puts the transparency of the device to an end. Under these circumstances, the only way to modify the color of the device is the use of dyes with different absorption spectra, which in turns causes a decrease of the cell efficiency. In the last years, similar limitations in rigid DSC based on either dyes or perovskite sensitizers have been overcome by means of integrating photonic crystal structures in the device.[14–28] In some of those cases, a boost of the efficiency as large as the one achievable with back diffuse scattering layers or by using scattering centers dispersed in the working electrode has been demonstrated.[29] At the same time, color fine-tuning, without modifying the sensitizer, and partial preservation of transparency were demonstrated. However, no approach of this sort, based on structural color, has been so far demonstrated for the flexible version of sensitized devices nor, more generally, in any flexible optoelectronic device, as most photonic structures present low-mechanical stability upon bending and stretching, which would negatively affect their performance.

Herein we demonstrate a synthetic route to integrate, for the first time, highly reflecting one dimensional photonic crystals (1DPCs) within working electrodes of flexible DSCs. We prove that they give rise to both an increase of the device power conversion efficiency (PCE) while keeping the possibility to see through them and endowing it with the structural color of choice. The mechanical strength of these flexible colored electrodes is confirmed by performing efficiency stability tests upon repeated bending of the device for more than a hundred times. All these features are of relevance for the application of 1DPC integrated flexible DSCs in BIPV. This work represents, to the best of our knowledge, the first example of integration of a bendable photonic structure into flexible optoelectronic

Dr. Y. Li, Dr. M. E. Calvo, Prof. H. Míguez
Instituto de Ciencia de Materiales de Sevilla
Consejo Superior de Investigaciones Científicas-Universidad de Sevilla
Calle Américo Vespucio 49
41092 Sevilla, Spain
E-mail: h.miguez@csic.es

DOI: 10.1002/adom.201500547

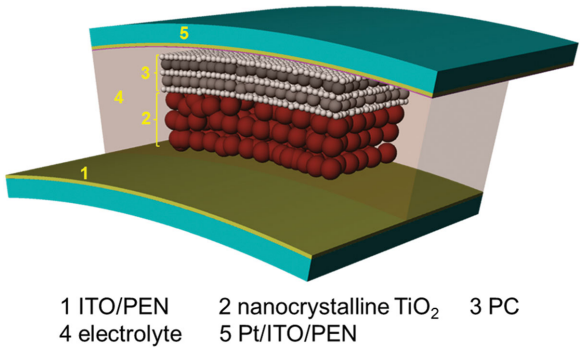

Figure 1. Schematic of 1DPC integrated flexible DSCs. The 1DPC, composing of individual layers of small TiO_2 and SiO_2, was deposited onto nanocrystalline TiO_2 (nc-TiO_2) with solution process. The substrates are plastics (PEN) with ITO conducting layer coated as working electrode and Pt/ITO coated at counter electrode. The 1DPC integrated nc-TiO_2 electrode was immersed in electrolyte, which was injected into the space between two flexible substrates.

devices, and opens the possibility to extend this same concept to other flexible photovoltaic technologies that may as well benefit from a more sophisticated optical design.

2. Results and Discussion

Figure 1 displays the scheme of the flexible DSC structure integrating a multilayer herein proposed. Our original hypothesis was that these multilayers would be able to resist bending of the cell without losing their optical quality, since we had already shown that it was possible to attain long-lasting self-standing flexible mirrors out of them.[30] This type of multilayers are made by sequentially stacking slabs of nanoparticles of different composition, namely SiO_2 and TiO_2, and size distribution, 30 ± 2 nm and 10 ± 2 nm, respectively.[31] They present photonic crystal properties and a void network through which fluids can easily diffuse,[32] which allow them to be used as highly reflecting porous mirrors that should not affect the charge transport along the DSC. In recent years, they have been integrated in rigid nanocrystalline titania electrodes prepared under basic conditions, as it has been reported before.[14,15,33] However, in the case of flexible DSCs, low-sintering temperature electrodes are prepared by a combination of low temperature chemical and physical sintering.[34–38] The surface of this electrode presents very different adhesion and mechanical properties than those employed to build rigid DSC. This implies that, in order to integrate photonic crystals on top of them, a series of challenges had to be overcome, such as the development of particle suspensions that were able to stick to the flexible nanocrystalline substrate. Full details can be found in the Experimental Section. Also they had to undergo the sintering-by-compression process without losing optical quality. As we will show next, nanoparticle multilayers showed all the required features for the goal herein pursued.

A set of 1DPCs reflecting different and well-defined wavelength ranges in the visible spectrum were spin-casted onto flexible TiO_2 photoelectrodes deposited onto plastic conducting substrates. The structure and morphology of their cross section was examined by scanning electron microscopy (SEM) images. Some examples are shown in **Figure 2**. As seen in Figure 2a, a uniform multilayer was deposited onto the surface of the photoanode. Higher magnification SEM pictures are shown in Figure 2b, where it can be seen that the average width of the bottom TiO_2 film is about 3.8 μm while the photonic crystal is, in this case, only 1 μm thick. A closer look at the individual layers composing the 1DPC, Figure 2c, allows us to estimate average thicknesses of 85 and 95 nm for the TiO_2 and SiO_2 layers, respectively. Please notice that the porous network observed in Figure 2c and Figure S1 in the Supporting Information permits the appropriate ionic diffusion of the electrolyte through the multilayer mirror. By using thicker TiO_2 and SiO_2 nanoparticle layers, the reflection of the integrated 1DPCs could be gradually changed from blue to red.

The optical reflectance and transmittance spectra of 1DPC based flexible electrodes were recorded before and after their physical compression and are depicted in **Figure 3**. The as-deposited photonic structures – that is, before physical compression – exhibited an intense reflection peak (≈75%) in the visible range. In the spectra chosen as examples, maximum reflectance (minimum transmittance) is attained at $\lambda = 640$ nm, $\lambda = 520$ nm, and $\lambda = 425$ nm, respectively, which correspond to red, green, and blue light reflecting multilayers. After physical compression, the maximum reflectance intensity increases up to ≈85% for all the photonic structures considered while, at the same time, their spectral position blueshifts (from $\lambda = 640$ nm to $\lambda = 585$ nm, from $\lambda = 520$ nm to $\lambda = 470$ nm, and from $\lambda = 425$ nm to $\lambda = 380$ nm, respectively). Both effects may be attributed to the densification of the TiO_2 and SiO_2 layers in the 1DPC, which should give rise to increased refractive index

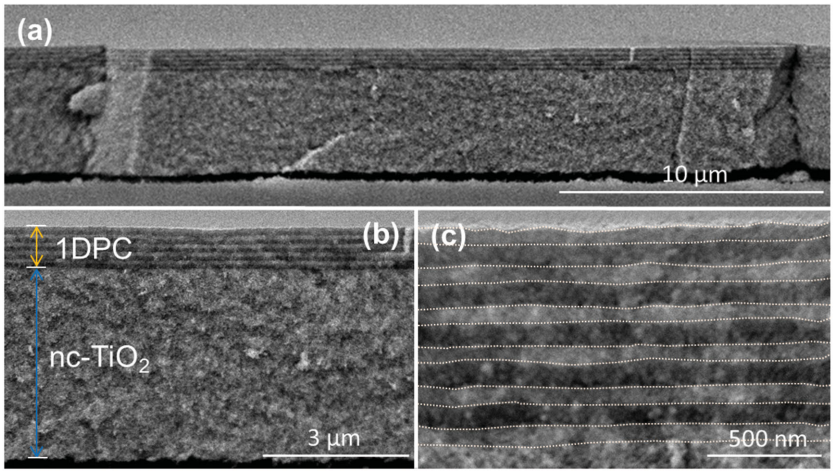

Figure 2. Scanning electron microscopy (SEM) images of as-prepared 1DPC/nanocrystalline TiO_2 film where the 1DPC is spin-coated with 5000 rpm. SEM with low magnification of 1DPC/TiO_2 film on flexible ITO/PEN substrate in (a). The enlarged SEM image of 1DPC with supporting TiO_2 film in (b) while the enlarged 1DPC films only where the interface of TiO_2 and SiO_2 layers are depicted with dash line in (c).

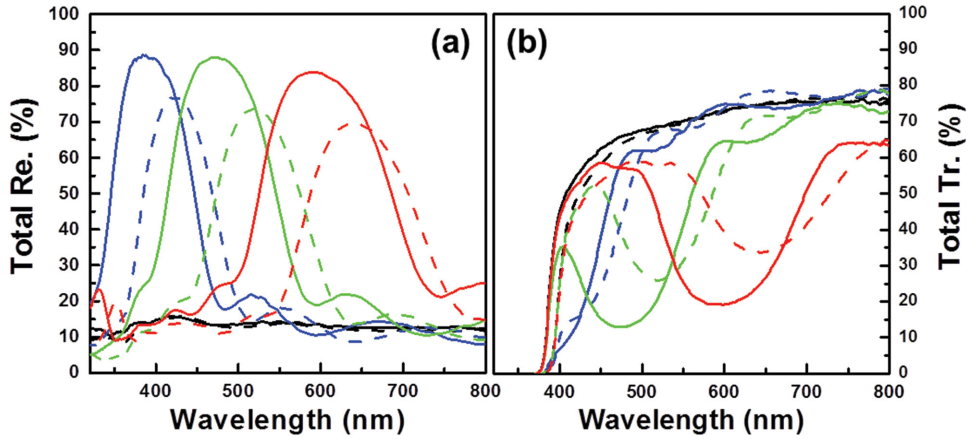

Figure 3. a) Total reflectance and b) total transmittance of 1DPC coated TiO_2 films. The black line stands for the reference TiO_2 film and the blue, green, and red ones for the different 1DPC coated TiO_2 films, respectively. Dashed and solid lines correspond to films measured before and after compressing them at 100 MPa for 3 min, respectively.

contrast between adjacent layers and to a shorter lattice constant. Meanwhile, it is also observed that the optical properties of the reference TiO_2 photoelectrode, that is, without introducing any photonic structure, show no significant changes before and after physical compression.

Once the electrode is dyed and the cell is sealed, the photonic structure gives rise to an intense color effect that depends strongly on the direction of incidence of the incoming light. **Figure 4** shows the spectral characterization of the light reflected (left panel) and transmitted (right panel) by a set of flexible cells containing different photonic crystals when light impinges from the front (solid lines) or from the back side (dashed lines). Pictures displayed in the central panel show the different colors observed with the naked eye for each cell under front and back illumination. This asymmetric optical response results from the total or partial suppression of frontal reflection of TiO_2 films integrating 1DPCs after being dye sensitized, an effect that is particularly strong for the case of blue and green-reflecting 1DPCs, whose reflectance peak coincides spectrally with the maximum of the absorption band of the ruthenium dye herein employed. The corresponding spectral drop observed in transmittance confirms that the frequencies back reflected by the porous dielectric mirror are being more efficiently absorbed as a result of the increased optical path of photons traveling within the photoanode. Contrarily, when cell irradiation takes place from the back side, light impinges on the photonic crystal before reaching the dyed nanocrystalline titania film and after passing only through the electrolyte and the counter electrode, whose absorption is much weaker than the dyed film. Hence, the color reflected by the multilayer is better preserved under rear illumination. A more detailed analysis of the effect of dying the electrodes coupled to photonic structures can be found in the Supporting Information (Figure S2). Please notice that the integration of a dielectric mirror implies not only that the cell may be endowed with the structural color of choice, but also that the transparency of the cell is partially maintained, as it can be inferred from the cell light transmission properties displayed in the right panel of Figure 4.

The effect of the colored mirrors on photovoltaic properties of flexible DSCs was analyzed by measuring the photocurrent-voltage (J–V) characteristics and the incident photon to current efficiency (IPCE), which are depicted in **Figure 5**. J–V curves were recorded under light intensity of one sun while IPCE was measured with a monochromated 300 W lamp. Both results are shown in Figure 5a,b, respectively. For comparison, reference cells made of TiO_2 photoelectrodes with the same thickness but without introducing 1DPCs were also prepared and characterized. As seen in Figure 5a, it can be readily observed that all 1DPCs integrated flexible DSCs demonstrated a significantly better photocurrent density (J_{SC}) than that of reference cells. As listed in **Table 1**, average J_{SC} increased from 6.09 mA cm^{-2} in reference DSCs to 6.85, 7.85, and 6.80 mA cm^{-2} for flexible cells integrating blue, green, and red reflecting mirrors, respectively. The maximum increment is achieved using green reflecting mirrors as back reflectors, which raised J_{SC} by approximately a 30%. At the same time, open circuit voltage (V_{OC}) of 1DPC integrated cells just exhibited a slight increase (≈5%) with respect to reference cells, an effect that has been reported before and attributed to the reduced recombination between photoinjected electrons in the conduction band of TiO_2 photoelectrode and oxidized species the electrolyte as a consequence of the formation of a very thin insulating layer around the TiO_2 nanocrystals forming the photoanode during the photonic crystal deposition process.[16] Simultaneously, fill factor (FF) deteriorates as the photonic crystal thickness increases, which may be attributed to retarded ionic diffusion of electrolyte through the small pore size multilayer. All relevant photovoltaic values are listed in Table 1. As a consequence of the fill factor decrease, the highest overall PCE is only an 18% higher than that attained from the reference cell. Nevertheless,

Table 1. Photovoltaic properties of flexible DSCs fabricated with 1DPC/TiO_2 films and reference TiO_2 films.

	J_{SC} [mA cm^{-2}]	V_{OC} [mV]	FF [%]	PCE [%]
Reference	6.09	710	63.8	2.76
Blue	6.85	714	59.4	2.91
Green	7.85	715	58.0	3.26
Red	6.80	718	58.3	2.85

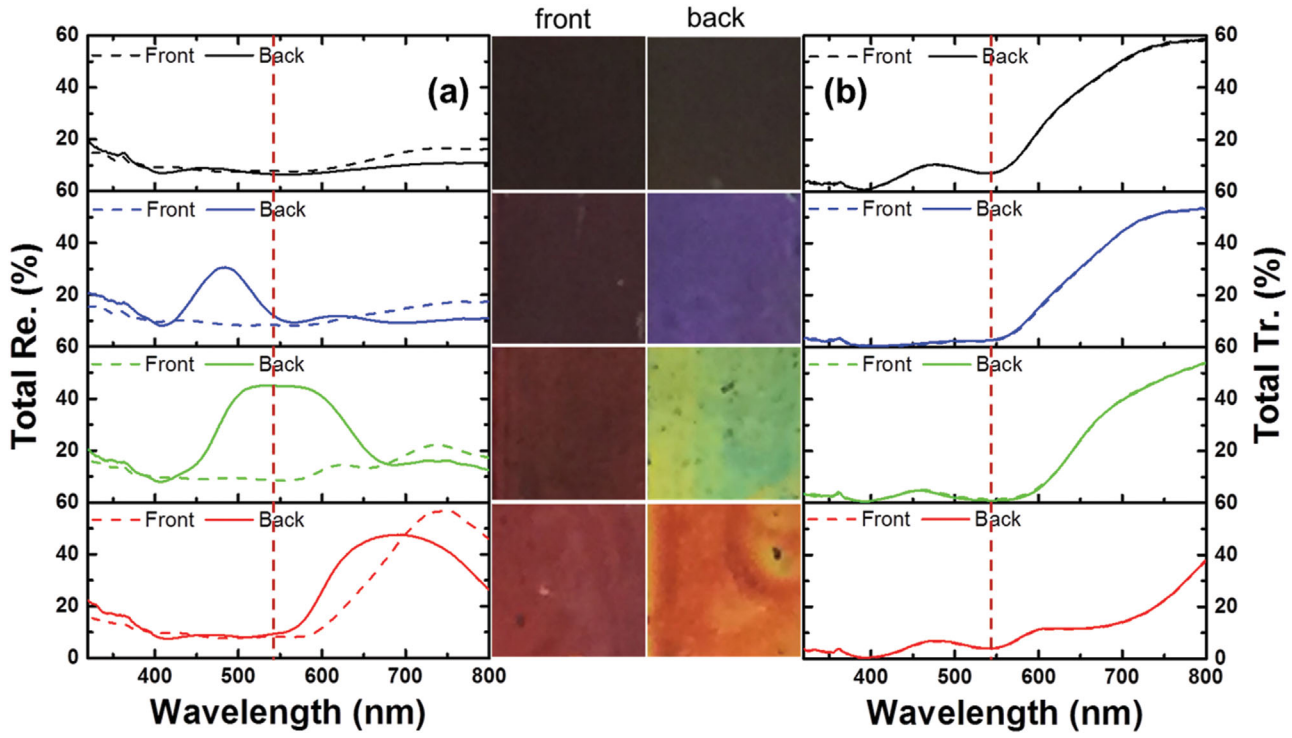

Figure 4. a) Total reflectance and b) total transmittance of both reference and 1DPC/TiO_2 film based cells. Different color lines are used for the reference cell (black line), and for cells in which the electrodes are coated with blue, green, and red light reflecting 1DPCs (blue, green, and red lines, respectively). The images taken from both front and back side of cells are presented on the right side of each plot. The vertical red dash line indicates the maximum absorption position of ruthenium dye.

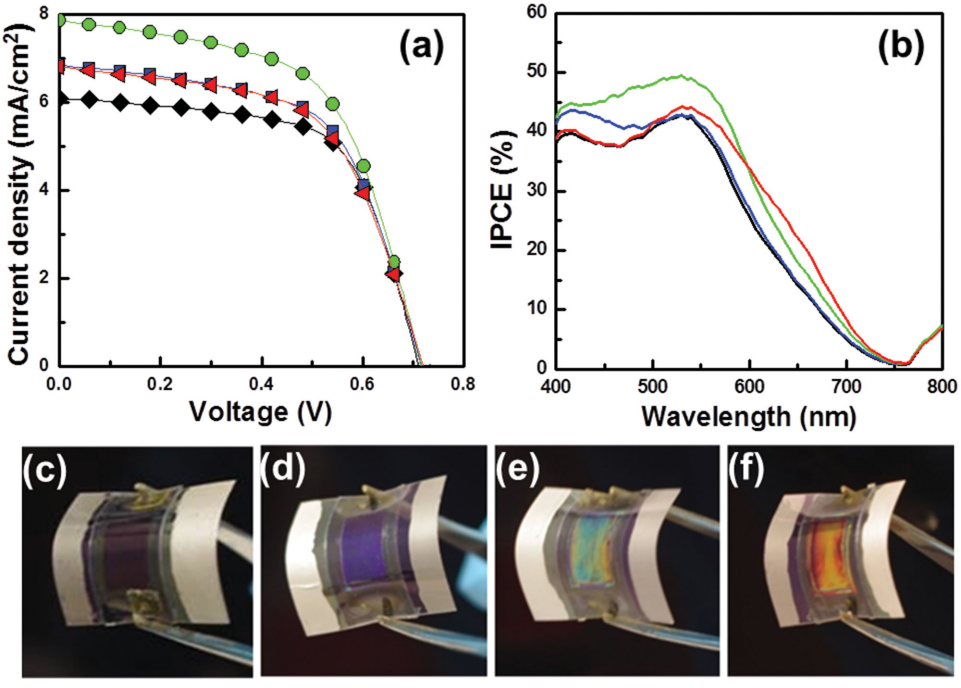

Figure 5. a) Photocurrent–voltage curves and b) IPCE of fully flexible cells prepared using a standard nanocrystalline TiO_2 film (black lines), and blue, green, and red light reflecting 1DPC coated TiO_2 films (blue, green, and red lines, respectively). The images of these flexible cells under bending are presented in (c)–(f).

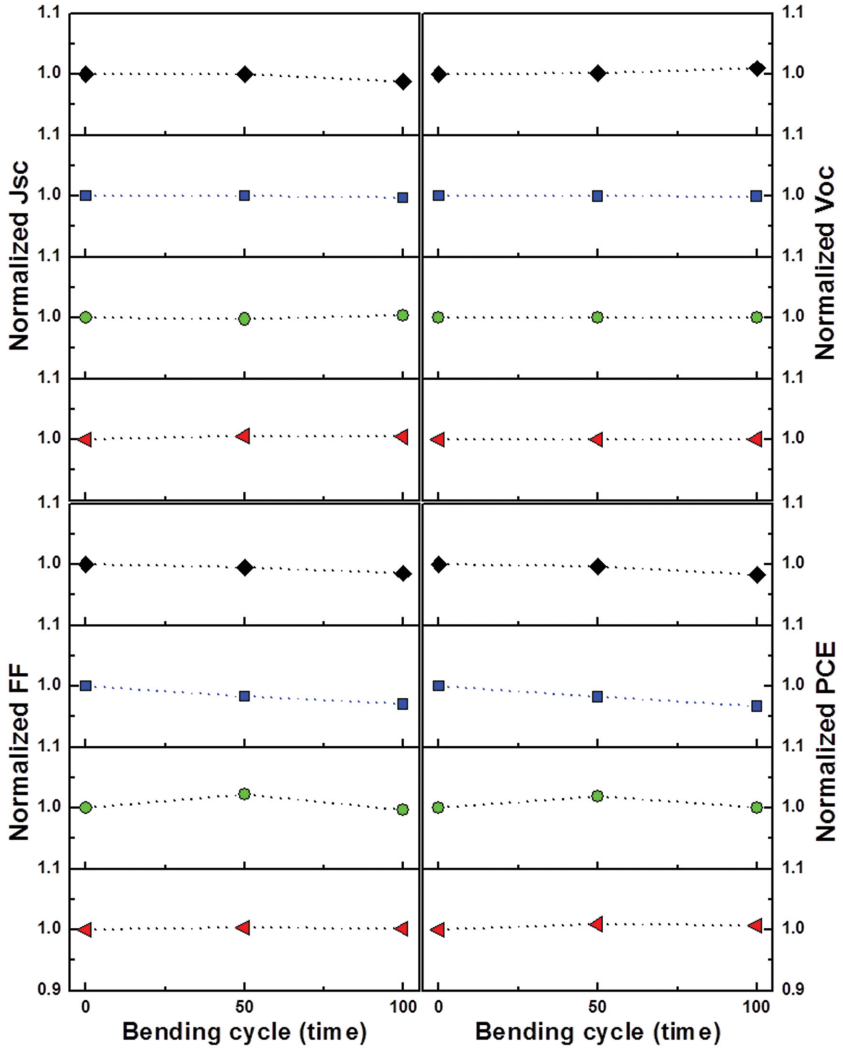

Figure 6. Photovoltaic performance of cells under repeated bending for 0, 50, and 100 times with bending radius of 14 mm. The J_{SC}, V_{OC}, FF, and PCE of cells are normalized by comparing with that before bending. Different color lines are used for the reference cell (black line), and for cells in which the electrodes are coated with blue, green, and red light reflecting 1DPCs (blue, green, and red lines, respectively).

these results confirm that, contrarily to what happens when any of the commonly employed diffuse scattering configurations is used,[14] the integration of photonic crystals allows enhancing the cell performance while preserving some of the features that make these devices attractive for the development of building integrated photovoltaic window or façade panes.

The analysis of the spectral dependence of the photogenerated current confirmed that the observed enhancement was caused by reinforced light harvesting taking place at those wavelength ranges for which the integrated multilayers present a stronger reflection. This can be clearly seen in the IPCE curves plotted in Figure 5b. Cells integrating blue, green, and red reflecting mirrors showed higher photocurrent in the 400 nm < λ < 520 nm, 400 nm < λ < 750 nm, and 500 nm < λ < 750 nm spectral ranges, respectively. The better performance of green reflecting back mirrors is due to the fact that the TiO_2 photoelectrode has a thickness of 3.8 µm, which is not enough to maximize light harvesting. In those cases, 1DPCs reflecting in the frequency range that overlaps with the absorption band of the sensitizer is capable of augmenting light harvesting more efficiently than red or blue reflectors, in good agreement with previous theoretical calculations.[39] In Figure 5c–f, pictures of a series of flexible cells displaying a wide color hue are depicted. Figure 5c corresponds to the original cell, without introducing any photonic structure, with the characteristic dark reddish color that results from the filtering of the spectrum of a white light source by the absorption spectrum of the ruthenium dye. Under illumination from the counter electrode side, 1DPC based flexible DSCs revealed bright reflection colors, as it can be seen in Figure 5d–f. Under frontal illumination, color differences are less noticeable as in this case light reflected by the mirror is used to increase the absorption of the photoanode, thus darkening even more the look of the cell.

The stability of the photonic structures was confirmed by monitoring the optical and photovoltaic properties of the flexible cells after undergoing a long series of uniaxial bends. Tests were performed at a constant strain by repeatedly putting into conformal contact the 1DPC-based cells with a cylindrical rod of radius 14 mm and then letting them go back to their initial flat shape. The normalized performance is presented in **Figure 6**, in which the result of dividing the specific photovoltaic parameter of choice, measured after a number of bends, by the starting value is plotted. As seen in Figure 6, J_{SC} and V_{OC} remain almost unchanged after bending and unbending the cell a hundred times, while FF presents a variation of 4%, which is probably due to changes induced in the resistance of the conducting substrate.[40] The overall PCE preserves above 96% of its initial value. At the same time, no modifications of the cell color were appreciable. Also, an analysis of the performance stability while 1DPC-based flexible cells were being bended was realized. In order to do so, *J*–*V* curves were measured for a set of 1DPC based cells at two different radius of curvature. Data normalized to the performance at infinite curvature radius (unbent cell) are plotted in **Figure 7**, where it can be observed that PCE slightly decreases down to a 96% of the original value for increasing bending of the cell. Eventually, 1DPC-based flexible cells recover their initial performance as they recuperate their straight shape. Finally, the dependence of the photovoltaic response with the incident angle of incoming light was also analyzed. The integration in a photovoltaic device of a photonic structure of the sort we employ here may originate a potentially strong anisotropic response. In order to evaluate the interplay of

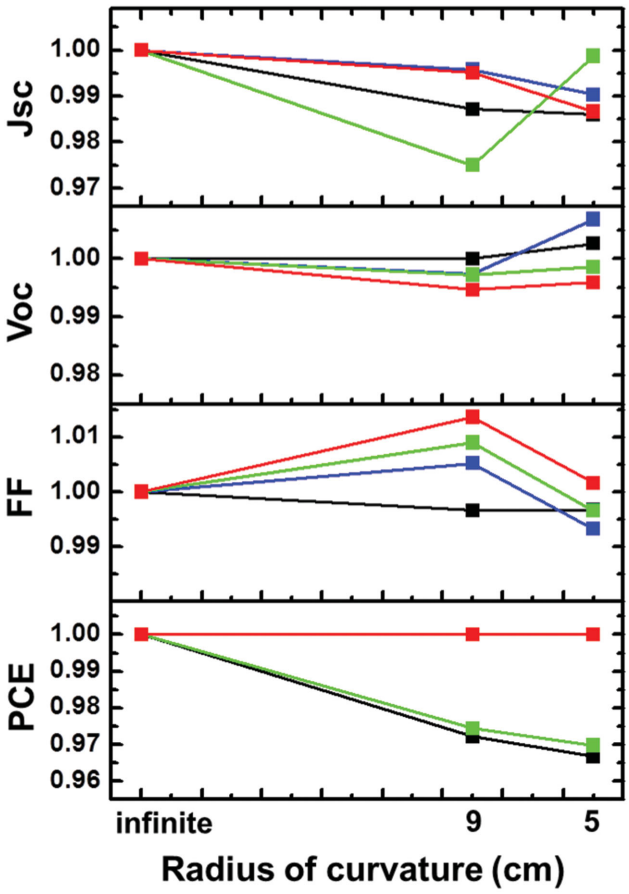

Figure 7. Photovoltaic performance of cells under bending status with varied bending radius of infinite, that is without bending, 9 and 5 cm. The J_{SC}, V_{OC}, FF, and PCE of cells are normalized by comparing with that without bending. Different color lines are used for the reference cell (black line), and for cells in which the electrodes are coated with blue, green, and red light reflecting 1DPCs (blue, green, and red lines, respectively). The PCE plots of blue and red reflecting cells are overlapped.

the incident angle of the solar radiation and the photovoltaic response, the cell performance was recorded by changing the incident angle of light from 0° to 60°, as shown in Figure S3 (Supporting Information). Similar results to those already reported for other rigid DSC integrating photonic crystals were attained, as expected.[33]

3. Conclusion

We have demonstrated for the first time that highly reflecting 1DPCs may be integrated in flexible optoelectronic devices. By depositing a porous multilayer mirror of high-mechanical stability onto a flexible photoanode, we were able to prove that light-harvesting efficiency can be reinforced while partially preserving the transparency of the cell, which is now endowed with the structural color of choice. The solar-to-electric conversion performance and appearance of the colored flexible device remains the same after repeated bending cycles. We believe all these features may allow the application of these versatile photonic structures into flexible DSCs with the aim of developing new products for building integration. This approach could in principle be equally applied to other flexible photovoltaic technologies, such as those based on perovskite or organic materials.

4. Experimental Section

Preparation and Characterization of the TiO_2 Electrode: TiO_2 nanoparticles with an average diameter of 20 nm were synthesized according to the procedure published previously.[41] An inorganic binding agent, TiO_2 nanoglue particles, with size of 5 nm was also prepared to formulate a viscous organic-binder-free TiO_2 paste for low-temperature coating.[42] Thin TiO_2 films with thickness of approximately 3.5 µm were coated from this organic-binder-free TiO_2 pastes onto plastic conducting substrates (ITO/PEN, Peccell, Japan) as supporting electrode for all cases. A 3M tape with thickness of about 60 µm was used as spacer to control the film thickness. After dried at ambient condition, these films were physically compressed at room temperature with pressure of 30 MPa (Specac Automatic Press). Surface of compressed TiO_2 films were further activated with oxygen plasma for 5 min (Diener Femto Plasma cleaner) before depositing photonic crystals.

Integration of One-Dimensional Photonic Crystals (1DPCs) with TiO_2 Electrodes: 1DPC structures were built by spin coating TiO_2 and SiO_2 nanoparticle suspensions on top of the compressed TiO_2 films. TiO_2 nanoparticles used for 1DPC were synthesized according to the procedure: 20 mL TTIP (97%, Aldrich) was dropwise added into 36 mL deionized H_2O (Milli-Q), and further vigorously stirred for 30 min. The resulted colloid was filtrated with 1.2 µm RTTP membrane filter (Isopore™ Membrane Filters, Millipore) and further rinsed by Milli-Q H_2O. The collected white powder was transferred into a Teflon container with 9.792 mL Mill-Q H_2O and 0.208 mL 65% nitric acid and further heated in a sealed stainless steel vessel at 160 °C for 18 h, which resulted in approximately 17 wt% colloid containing particles of nanocrystalline anatase with an average diameter of 7.5 nm. In order to prepare the 1DPC onto compressed TiO_2 films, 17 wt% TiO_2 based colloids was further diluted to 2 wt% and 3 wt% suspension by adding certain amount of methanol. SiO_2 nanoparticles (average diameter of 30 nm) were purchased from Dupont (34 wt% suspension in H_2O, LUDOX TMA) and diluted to 2 wt% SiO_2 by adding methanol. Surface activation of compressed TiO_2 films was performed by oxygen plasma before spin coating the 1DPC. The periodic structure was then fabricated by stacking 11 alternate layers made of such suspensions using a spin coater (Laurell WS-400E-6NPP-LITE) working at various speed with an acceleration of 10260 rpm s^{-1}. The first and last layers were deposited from the TiO_2 dispersion. To prepare the 1DPCs reflecting at different wavelength ranges, the rotation speed of the spin coating and the concentration of TiO_2 nanoparticles in the suspension was slightly varied, for instance, 2 wt% TiO_2 suspension and 7000 rpm were used to attain a blue-reflecting 1DPC, 3 wt% and 5000 rpm for making a green-reflecting 1DPC, and 3 wt% and 3000 rpm to build a red-reflecting 1DPC. Finally, all samples were physically compressed at room temperature with pressure of 100 MPa (Specac Automatic Press) before dye adsorption.

Fabrication of Flexible Dye Solar Cell (DSCs): PC integrated TiO_2 films were completely immersed in 0.5×10^{-3} M N719 dye solution in anhydrous ethanol for 12 h (Everlight, Taiwan). After immersion, the dye-sensitized TiO_2 films were rinsed by anhydrous ethanol and dried by N_2 flow, which were used as working electrodes later. For fully flexible cells, a flexible counter electrode of Pt/ITO/PEN substrate (Peccell, Japan) was used. Both electrodes were then assembled by a thermoplastic film (Surlyn, 25 µm, Solaronix). A drop of electrolyte with composition of 0.4 M tetrabutylammonium iodide (TBAI), 0.1 M lithium iodide (LiI), 0.02 M iodine (I_2), 0.5 M 4-tert-butylpyridine (tBP) using anhydrous acetonitrile as solvent, was injected through the holes drilled on the counter electrode. Reference DSCs were made using TiO_2

electrodes of the same thickness but without coupling any photonic structures on top.

Optical and Photovoltaic Characterization: Total reflectance and total transmittance spectra of 1DPC integrated TiO_2 films or cells were obtained using an integrating sphere attached to an UV–visible scanning spectrophotometer (SHIMADZU UV-2101PC). Photocurrent-voltage characterization was performed with a digital sourcemeter (Keithley 2400) coupled solar simulator (Sun 2000, Abet Technologies) including a 150 W arc xenon lamp and the appropriate filter to replicate the AM1.5 solar spectrum. The black mask with a proper aperture was attached onto cells to get rid of effect of diffused light. The incident light intensity was confirmed to be 100 mW cm^{-2} using certificated silicon solar cells. Incident photon to collected electron (IPCE) efficiency measurements were acquired using a home-built system composed of a 300 W xenon lamp, a monochromator with 1140 g mm^{-1} grating (Model 272, McPherson) controlled by a digital scan drive system (Model 789A-3, McPherson), and a picoammeter (Keithley 6485). A calibrated silicon photodiode (D8-Si-100 TO-8 Detector, Sphere Optics) was used to correct the cell response. A UV filter with cut-off wavelength at 400 nm was used to get rid of the second order harmonics exiting the monochromator.[16,33]

In order to perform the angular measurements, a sample holder was attached to a rotating stage, with an angular scale resolution of 10 arc min. In this study, it is zero degree for the case of light incidence normal to the cell surface. A black mask with a proper aperture was used to cover the TiO_2 electrode and its lateral sides to prevent diffused light, which might largely change the cell response and give rise to erroneous interpretations.

In order to investigate the mechanical stability of the 1DPC coupled flexible dye cells, a uniaxial bending test with a constant strain was repeated using a cylindrical rod with a known radius of 14 mm. The cell performance was measured before and after 50 and 100 bending cycles.[40,43] Photovoltaic properties were also measured for various bending radius using the same method.

Supporting Information

Supporting Information is available from the Wiley Online Library or from the author.

Acknowledgements

Financial support of the European Research Council under the European Union's Seventh Framework Programme (FP7/2007–2013)/ERC Grant agreement No. 307081 (POLIGHT) and the Spanish Ministry of Economy and Competitiveness under Grant No. MAT2014-54852-R is gratefully acknowledged. Y.L. acknowledges the financial support from the People Programme (Marie Curie Actions) of the European Union's Seventh Framework Programme FP7/2007-2013/under REA Grant agreement No. 622533.

Received: September 29, 2015
Revised: October 21, 2015
Published online: December 16, 2015

[1] M. Pagliaro, G. Palmisano, R. Ciriminna, *Flexible Solar Cells*, Wiley-VCH Verlag GmbH & Co. KGaA, Weinheim **2008**.
[2] S.-M. Lee, R. Biswas, W. Li, D. Kang, L. Chan, J. Yoon, *ACS Nano* **2014**, *8*, 10507.
[3] A. Chirilă, S. Buecheler, F. Pianezzi, P. Bloesch, C. Gretener, A. R. Uhl, C. Fella, L. Kranz, J. Perrenoud, S. Seyrling, R. Verma, S. Nishiwaki, Y. E. Romanyuk, G. Bilger, A. N. Tiwari, *Nat. Mater.* **2011**, *10*, 857.
[4] J. Jean, P. R. Brown, R. L. Jaffe, T. Buonnassisi, V. Bulovic, *Energy Environ. Sci.* **2015**, *8*, 1200.
[5] B. Kippelen, J.-L. Brédas, *Energy Environ. Sci.* **2009**, *2*, 251.
[6] B. J. Kim, D. H. Kim, Y.-Y. Lee, H.-W. Shin, G. S. Han, J. S. Hong, K. Mahmood, T. K. Ahn, Y.-C. Joo, K. S. Hong, N.-G. Park, S. Lee, H. S. Jung, *Energy Environ. Sci.* **2015**, *8*, 916.
[7] K. Yoo, J.-Y. Kim, J. A. Lee, J. S. Kim, D.-K. Lee, K. Kim, J. Y. Kim, B. Kim, H. Kim, W. M. Kim, J. H. Kim, M. J. Ko, *ACS Nano* **2015**, *9*, 3760.
[8] Z. Fan, H. Razavi, J.-w. Do, A. Moriwaki, O. Ergen, Y.-L. Chueh, P. W. Leu, J. C. Ho, T. Takahashi, L. A. Reichertz, S. Neale, K. Yu, M. Wu, J. W. Ager, A. Javey, *Nat. Mater.* **2009**, *8*, 648.
[9] I. J. Kramer, G. Moreno-Bautista, J. C. Minor, D. Kopilovic, E. H. Sargent, *Appl. Phys. Lett.* **2014**, *105*, 163902.
[10] W. Guo, X. Zhang, R. Yu, M. Que, Z. Zhang, Z. Wang, Q. Hua, C. Wang, Z. L. Wang, C. P. Pan, *Adv. Energy. Mater.* **2015**, *5*, 1500141.
[11] M. J. Yun, S. I. Cha, S. H. Seo, D. Y. Lee, *Sci. Rep.* **2014**, *4*, 5322.
[12] T. Miyasaka, *J. Phys. Chem. Lett.* **2011**, *2*, 262.
[13] S. Ito, N.-L. C. Ha, G. Rothenberger, P. Liska, P. Comte, S. M. Zakeeruddin, P. Pechy, M. K. Nazeeruddin, M. Gräetzel, *Chem. Commun.* **2006**, 4004.
[14] S. Colodrero, A. Mihi, L. Haggman, M. Ocana, G. Boschloo, A. Hagfeldt, H. Míguez, *Adv. Mater.* **2009**, *21*, 764.
[15] S. Colodrero, A. Forneli, C. López-López, L. Pelleja, H. Míguez, E. Palomares, *Adv. Funct. Mater.* **2012**, *22*, 1303.
[16] D. Colonna, S. Colodrero, H. Lindstrom, A. Di Carlo, H. Míguez, *Energy Environ. Sci.* **2012**, *5*, 8238.
[17] W. Zhang, M. Anaya, G. Lozano, M. E. Calvo, M. B. Johnston, H. Míguez, H. J. Snaith, *Nano Lett.* **2015**, *15*, 1698.
[18] A. Mihi, C. J. Zhang, P. V. Braun, *Angew. Chem. Int. Ed.* **2011**, *50*, 5711.
[19] M. Guo, Z. Yong, K. Xie, J. Lin, Y. Wang, H. Huang, *ACS Appl. Mater. Interfaces* **2013**, *5*, 13022.
[20] S. Guldin, S. Huttner, M. Kolle, M. E. Welland, P. Muller-Buschbaum, R. H. Friend, U. Steiner, N. Tetreault, *Nano Lett.* **2010**, *10*, 2303.
[21] S. Foster, S. John, *Energy Environ. Sci.* **2013**, *6*, 2972.
[22] J. T. Park, J. H. Prosser, S. H. Ahn, S. J. Kim, J. H. Kim, D. Lee, *Adv. Funct. Mater.* **2013**, *23*, 2193.
[23] D.-K. Hwang, B. Lee, D.-H. Kim, *RSC Adv.* **2013**, *3*, 3017.
[24] M. Guo, K. Xie, J. Lin, Z. Yong, C. T. Yip, L. Zhou, Y. Wang, H. Huang, *Energy Environ. Sci.* **2012**, *5*, 9881.
[25] C. T. Yip, H. Huang, L. Zhou, K. Xie, Y. Wang, T. Feng, J. Li, W. Y. Tam, *Adv. Mater.* **2011**, *23*, 5624.
[26] M. Guo, K. Xie, Y. Wang, L. Zhou, H. Huang, *Sci. Rep.* **2014**, *4*, 6642.
[27] L.-P. Heiniger, P. G. O'Brien, N. Soheilnia, Y. Yang, N. P. Kherani, M. Gräetzel, G. A. Ozin, N. Tetreault, *Adv. Mater.* **2013**, *25*, 5734.
[28] M. Guo, K. Xie, X. Liu, Y. Wang, L. Zhou, H. Huang, *Nanoscale* **2014**, *6*, 13060.
[29] C. López-López, S. Colodrero, H. Míguez, *Phys. Chem. Chem. Phys.* **2014**, *16*, 663.
[30] J. R. Castro Smirnov, M. E. Calvo, H. Míguez, *Adv. Funct. Mater.* **2013**, *23*, 2805.
[31] S. Colodrero, M. Ocana, H. Míguez, *Langmuir* **2008**, *24*, 4430.
[32] C. López-López, S. Colodrero, S. R. Raga, H. Lindström, F. Fabregat-Santiago, J. Bisquert, H. Míguez, *J. Mater. Chem.* **2012**, *22*, 1751.
[33] C. López-López, S. Colodrero, M. E. Calvo, H. Míguez, *Energy Environ. Sci.* **2013**, *6*, 1260.

[34] Y. Li, K. Yoo, D.-K. Lee, J. Y. Kim, H. J. Son, J. H. Kim, C.-H. Lee, H. Míguez, M. J. Ko, *RSC Adv.* **2015**, *5*, 76795.
[35] T. Yamaguchi, N. Tobe, D. Matsumoto, T. Nagai, H. Arakawa, *Sol. Energ. Mater. Sol. Cells* **2010**, *94*, 812.
[36] N. G. Park, K. M. Kim, M. G. Kang, K. S. Ryu, S. H. Chang, Y. J. Shin, *Adv. Mater.* **2005**, *17*, 2349.
[37] H. C. Weerasinghe, G. V. Franks, J. D. Plessis, G. P. Simon, Y.-B. Cheng, *J. Mater. Chem.* **2010**, *20*, 9954.
[38] Y. Li, W. Lee, D. K. Lee, K. Kim, N. G. Park, M. J. Ko, *Appl. Phys. Lett.* **2011**, *98*, 103301.
[39] G. Lozano, S. Colodrero, O. Caulier, M. E. Calvo, H. Míguez, *J. Phys. Chem. C* **2010**, *114*, 3681.
[40] Y. Li, D.-K. Lee, J. Y. Kim, B. Kim, N.-G. Park, K. Kim, J.-H. Shin, I.-S. Choi, M. J. Ko, *Energy Environ. Sci.* **2012**, *5*, 8950.
[41] A. Zaban, S. Ferrere, J. Sprague, B. A. Gregg, *J. Phys. Chem. B* **1997**, *101*, 55.
[42] Y. Li, K. Yoo, D.-K. Lee, J. Y. Kim, H. Kim, B. Kim, M. J. Ko, *Nanoscale* **2013**, *5*, 4711.
[43] Y. Li, K. Yoo, D. K. Lee, J. H. Kim, N. G. Park, K. Kim, M. J. Ko, *Curr. Appl. Phys.* **2010**, *10*, E171.